rf Absorption and Ion Heating in Helicon Sources

J. L. Kline, E. E. Scime, R. F. Boivin, A. M. Keesee, and X. Sun

Department of Physics, West Virginia University, Morgantown, West Virginia 26505

V. S. Mikhailenko

Kharkiv National University, Kharkiv, Ukraine 61002

Experimental data are presented that are consistent with the hypothesis that anomalous rf absorption in helicon sources is due to electron scattering arising from parametrically driven ion-acoustic waves downstream from the antenna. Also presented are ion temperature measurements demonstrating anisotropic heating ($T_\perp > T_\parallel$) at the edge of the discharge. The most likely explanation is ion-Landau damping of electrostatic slow waves at a local lower-hybrid-frequency resonance.

Since the late 1980's, the mechanism responsible for the high rf absorption efficiency of helicon plasma sources has been the subject of both theoretical and experimental investigations. In his initial series of publications describing the helicon source, Boswell presented measurements of plasma density versus magnetic field strength and fluctuating magnetic field profiles that were consistent with the excitation of bounded whistler waves [1,2], i.e., helicon waves [3]. However, calculations showed that collisional damping of helicon waves, particularly at low neutral pressures, was insufficient to explain the high rf absorption efficiency of helicon sources [4]. Chen suggested that Landau damping of energetic electrons could be responsible for the high rf absorption efficiency [4]. Since then, experimental measurements suggestive of energetic electrons in helicon sources have been reported [5–8]. Recent measurements suggest that the upper limit on the number of energetic electrons in a helicon plasma is well below the minimum number required for Landau damping to play a significant role in rf power absorption [9]. However, those measurements may not be applicable to helicon sources operating at higher powers and weaker magnetic fields [10]. Chen and Blackwell also reported that the measured resistive loading of the rf antenna was consistent with coupling to strongly damped, electrostatic, slow waves at the plasma edge [9].

Alternatively, the excitation of ion-acoustic parametric turbulence by the primary rf wave in helicon plasmas has been suggested as a possible mechanism for heating electrons and coupling rf power into the plasma [11]. Since typical helicon source plasmas are not fully ionized, increased electron heating yields increased ionization and therefore larger plasma densities. The exact location of the ion-acoustic turbulence region depends on the amplitude of the rf wave, the electron density, and the electron temperature [11]. For typical experimental values, the theory predicts an enhanced density region a few tens of centimeters away from the antenna [11]. The observed location of downstream density peaks and the measured damping rate of the helicon wave in helicon sources are consistent with the predictions of the ion-acoustic turbulence model [12].

In this Letter, we present experimental evidence of electron heating correlated with parametrically driven electrostatic waves generated downstream from the antenna in a helicon plasma source. We also present experimental evidence of anisotropic ion heating in the edge of a helicon source. The range of rf frequencies and magnetic fields at which the ion heating occurs is consistent with Landau damping of the so-called slow or "Trivelpiece-Gould waves" on the ions.

In contrast to our previous experiments, which were all performed in glass vacuum chambers [13,14], these experiments were performed in a hybrid metal-glass chamber (Fig. 1). The rf antenna is mounted on the outside of the 10-cm-diam Pyrex section of the chamber. Laser induced fluorescence [15] was used to non-invasively measure the ion temperature at positions A, B, and C, in Fig. 1 ($z = 66.0$, 35.5, and 4.5 cm as measured from the left edge of the antenna). The density and electron temperature were determined at $z = 35.5$ cm with an rf-compensated Langmuir probe [16] and confirmed by microwave interferometry at $z = 66.0$ cm [17]. An uncompensated double
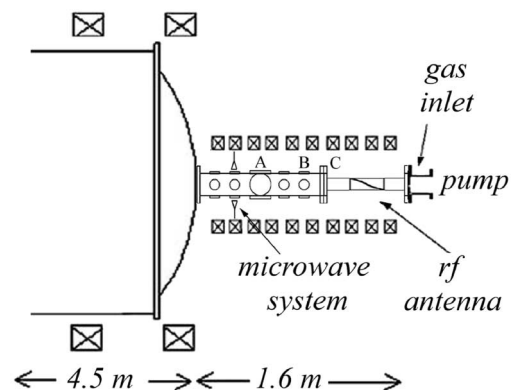
FIG. 1. The 19 cm helical antenna is wrapped around the outside of a 10 cm o.d. Pyrex tube. The remainder of the source vacuum vessel is a 15.25 cm o.d. stainless steel chamber. At the end of the source chamber is a 4.5-m-long, 2 m o.d. expansion chamber. Measurements were performed at locations A, B, and C, as indicated in the text.

probe at $z = 35.5$ cm was used to measure high-frequency electrostatic fluctuations. The double probe has tips of 0.5-mm-diam graphite and a spacing of 5 mm. The rf power was 750 W, the neutral gas pressure was 6.7 mTorr, the ion species was argon, and a 19-cm-long helical antenna was used [13]. To permit operation at magnetic fields of up to 1300 G, the two leftmost source region electromagnets in Fig. 1 are disconnected and the magnetic field diverges sharply after the eighth coil. The magnetic field in the expansion chamber at the end of the source was held constant at 36 G. Visual cues (the helicon plasma "blue-core") and measurements of the parallel wave number of the rf wave indicated that all of the experiments reported here were performed in helicon mode plasmas [18].

The electron temperature, electron density, and perpendicular ion temperature at $z = 35.5$ cm as a function rf frequency and magnetic field strength are shown in Fig. 2. Also shown in Fig. 2 are curves indicating where the rf frequency equals the on-axis lower hybrid frequency, $1/\omega_{LH}^2 \cong 1/(\omega_{pi}^2 + \omega_{ci}^2) + 1/(\omega_{ce}\omega_{ci})$. ω_{ce} and ω_{ci} are the electron and ion cyclotron frequencies and ω_{pi} is the ion plasma frequency. For typical plasma densities at the center of the discharge, the ion plasma frequency term is ignorable and $\omega_{LH}(0) \cong \sqrt{\omega_{ce}\omega_{ci}}$. Looking from left to right in Fig. 2a, there is a clear increase in electron temperature as the rf frequency nears the lower hybrid frequency. Initial analysis of the Langmuir probe data in the $\omega < \omega_{LH}(0)$ region, the lower right corner of the figure, suggests that the continued increase in electron temperature seen in Fig. 2a results from the appearance of a net drift in the electron distribution function and not from a true increase in electron temperature [19].

For rf frequencies from 8 to 12.5 MHz, the largest plasma densities occur for $\omega \approx \omega_{LH}$. Above 12.5 MHz,

there is a small region of increased plasma density that extends to weaker magnetic fields. Profile measurements indicate that, for $\omega \approx \omega_{LH}$, the density profile is peaked on axis. Other groups have also reported a correlation between the lower hybrid frequency and density production in helicon sources [20–22]. That the magnitude of the density peak at $\omega \approx \omega_{LH}$ depends on the choice of rf frequency and magnetic field strength (see the density data near 12 MHz and 1100 G) suggests that eigenmode resonances may also play an important role in coupling rf power into helicon sources [22].

The frequency spectrum of electrostatic waves as measured by a single tip of the double probe is shown in Fig. 3a for three rf frequencies and a magnetic field of 1 kG (parameters identified by i, ii, and iii in Fig. 2b). All three spectra have features typical of kinetic parametric instabilities [11] and quasimode (linear), parametric decay [23,24]: distinct sidebands about the rf pump wave with more power in the sidebands at frequencies below the pump wave than above, a low-frequency "beat" wave such that $\omega_{low} + \omega_{sideband} = \omega_{rf}$, and wave numbers that satisfy $k_{low} + k_{sideband} = k_{rf}$ (confirmed by phase difference measurements). In addition to the sidebands, for the 11 MHz case there is a broad spectral feature extending from 8 to 12 MHz. The frequency spacing between the sidebands and the pump wave, the amplitude of the sidebands, and the amplitude of the broad spectral feature are greatest for the 11 MHz case; the conditions at which the rf frequency is closest to the on-axis lower hybrid frequency. The amplitude of the low-frequency features and the plasma densities are similar for the 11 and 13.5 MHz cases. Frequency spectra as a function of radius are shown in Fig. 3b. The amplitudes of the sidebands, the broadband feature, and the low-frequency beat wave all increase
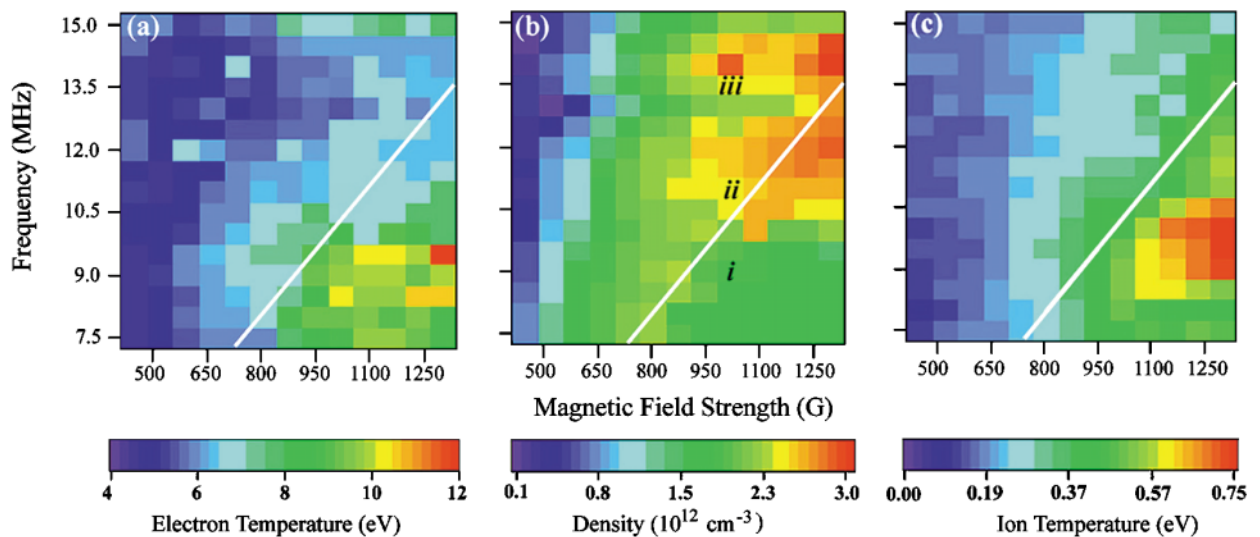
FIG. 2 (color). (a) electron temperature, (b) plasma density, and (c) ion temperature versus rf frequency and magnetic field strength at $z = 35.5$ cm. The white line indicates where the rf frequency equals the on-axis lower hybrid frequency. The black Roman numerals indicate particular combinations of rf frequency and magnetic field strength referred to in the text.
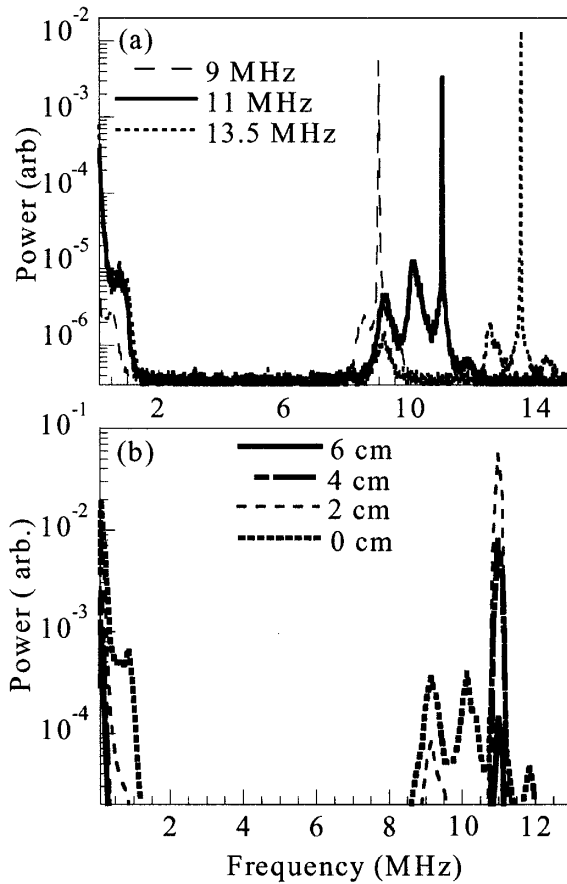
FIG. 3. (a) Power spectrum of electrostatic fluctuations for three different rf frequencies. (b) Power spectrum of electrostatic fluctuations versus radius. The rf frequency was 11 MHz and the magnetic field was 737 G.

FIG. 4 (color). (a) Ion temperature versus rf frequency and magnetic field strength at $z = 4.5$ cm. (b) Difference in ion temperature between $z = 4.5$ cm and $z = 35.5$ cm versus rf frequency and magnetic field strength. The color bar is the same as for Fig. 2c.

towards the center of the discharge. Note that a clear low-frequency beat wave appears in Fig. 3b only on axis. Electrostatic power spectrum measurements at $z = 66.0$ cm showed no evidence of either sidebands or broadband features.

As shown in Fig. 2c, the perpendicular ion temperature at $z = 35.5$ cm peaks for $\omega < \omega_{LH}(0)$. Near the antenna, $z = 4.5$ cm, the peak perpendicular ion temperature is a factor of 2 smaller (Fig. 4a). Figure 4b shows the difference in ion temperature between $z = 35.5$ and $z = 4.5$ cm. For $\omega > \omega_{LH}(0)$, the perpendicular ion temperature is relatively constant along the axis of the source. For $\omega < \omega_{LH}(0)$, an additional ion heating mechanism adds energy to the ions a few tens of centimeters downstream of the antenna. Therefore, like the plasma density in a helicon source [16], the maximum perpendicular ion temperature occurs downstream from the antenna (ion-temperature measurements at $z = 66.0$ are similar to those at $z = 4.5$ cm).

Radial profiles of the perpendicular and parallel ion temperature at $z = 35.5$ cm and for the plasma conditions indicated by an asterisk in Fig. 4b (9 MHz and 1200 G) are

shown in Fig. 5. The perpendicular ion temperature is constant across the inner portion of the discharge and increases at the edge. To create a perpendicular ion-temperature profile that is flat or increases at the edge, the ions must be heated anisotropically at the edge of the plasma or the heat conductivity along the axis must be extremely large. Since the perpendicular ion temperature varies with axial position, i.e., the parallel ion thermal conductivity is not large, the most likely explanation for the profile measurements is strong perpendicular ion heating at the edge. The parallel ion-temperature profile is similar to the plasma density profile. Thus, parallel ion heating likely arises from collisional isotropization of the ion temperature. Similar ion-temperature profiles are observed throughout the enhanced heating region shown in Fig. 4b.

In the low-density edge plasma, the "fast" or helicon wave cannot propagate. However, the slow wave branch of the cold plasma dispersion relationship can propagate [22].
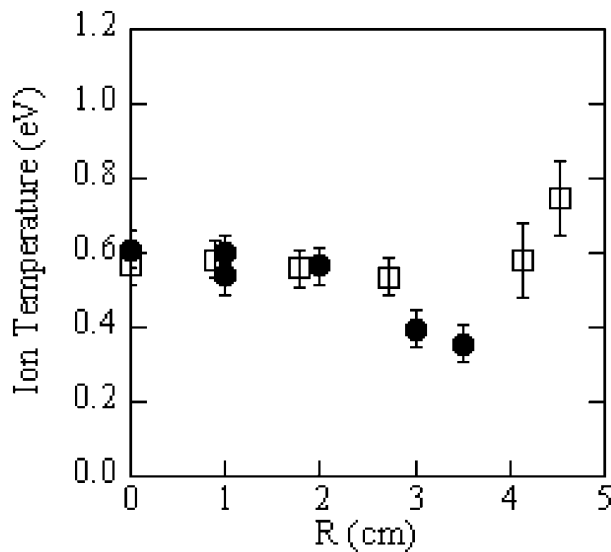
FIG. 5. Perpendicular (open squares) and parallel (filled circles) ion temperature versus radius for an rf frequency of 9 MHz and a magnetic field of 1200 G.

When the rf wave frequency equals the local lower hybrid frequency, the slow wave becomes predominately electrostatic and the perpendicular wave number of the wave goes to infinity in a collisionless plasma [22]. Because of the low plasma densities near the plasma edge (as measured with the Langmuir probe), the local lower hybrid frequency can drop below 8 MHz even though the lower hybrid frequency on axis is 12 MHz. At large perpendicular wave numbers, $k_\perp \sim 600$ cm^{-1}, the wave phase velocity is low enough that ion-Landau damping can occur. For the region of rf frequencies and magnetic field strengths at which the enhanced ion heating occurs in Fig. 4b, the formalism of Ref. [22] yields slow wave perpendicular wave numbers sufficiently large to result in ion-Landau damping. For different rf frequencies and magnetic field strengths, the calculations yield much smaller perpendicular wave numbers. Consistent with the temperature profile measurements, the calculated perpendicular wave numbers (for our measured density profiles) are largest at the edge of the plasma. We note that similar results were obtained during slow wave lower hybrid ion heating experiments in other types of discharges [23].

In summary, for $\omega < \omega_{LH}(0)$, the measurements suggest that enhanced ion heating in helicon sources results from ion-Landau damping of slow waves in the edge region of the source. Damping of the low-frequency beat waves seen in Fig. 3 is unlikely to be the cause of the ion heating since the low-frequency beat waves appear only near the center of the discharge (Fig. 3b). Detailed measurements and calculations of wavelengths in the edge during intense ion heating will be presented in a future paper. In addition, the electron temperature and plasma density increase substantially for frequencies near the lower hybrid frequency. Given the simultaneous appearance of low-frequency ion-acoustic-like waves and spectral features typical of parametric decay, it appears that parametrically driven ion-acoustic waves and/or ion-acoustic turbulence plays an important role in rf power absorption through increased electron scattering. Finally, we also note that parametric decay of large amplitude whistler waves correlated with anomalous particle heating has been observed in other linear devices [24]

[1] R. W. Boswell, Phys. Lett. **25A**, 457 (1970).
[2] R. W. Boswell, Aust. J. Phys. **25**, 403 (1972).
[3] H. A. Blevin and P. J. Christiansen, Plasma Phys. Controlled Fusion **10**, 779 (1968).
[4] F. F. Chen, Plasma Phys. Controlled Fusion **33**, 339 (1991).
[5] Z. Peiyuan and R. W. Boswell, J. Appl. Phys. **68**, 1981 (1990).
[6] A. R. Ellingboe, R. W. Boswell, J. P. Booth, and N. Sadeghi, Phys. Plasmas **2**, 1807 (1995).
[7] A. W. Molvik, A. R. Ellingboe, and T. D. Rognlien, Phys. Rev. Lett. **79**, 233 (1997).
[8] R. T. S. Chen and N. Hershkowitz, Phys. Rev. Lett. **82**, 2677 (1999).
[9] A. I. Akhiezer, V. S. Mikhailenko, and K. N. Stepanov, Phys. Rev. Lett. **245**, 117 (1998).
[10] F. F. Chen and D. D. Blackwell, Phys. Rev. Lett. **82**, 2677 (1999).
[11] G. Gozadinos, M. M. Turner, and D. Vender, Phys. Rev. Lett. **87**, 135004 (2001).
[12] I. D. Sudit and F. F. Chen, Plasma Sources Sci. Technol. **5**, 43 (1996).
[13] M. Balkey, R. Boivin, P. Keiter, J. Kline, and E. Scime, Plasma Sources Sci. Technol. **10**, 284 (2001).
[14] J. Kline, E. Scime, P. Keiter, M. Balkey, and R. Boivin, Phys. Plasmas **6**, 4767 (1999).
[15] E. E. Scime *et al.*, Plasma Sources Sci. Technol. **7**, 186 (1998).
[16] I. D. Sudit and F. F. Chen, Plasma Sources Sci. Technol. **3**, 162 (1994).
[17] E. E. Scime, R. F. Boivin, J. L. Kline, and M. M. Balkey, Rev. Sci. Instrum. **72**, 1672 (2001).
[18] A. Ellingboe and R. Boswell, Phys. Plasmas **2**, 2797 (1996).
[19] T. Sheridan and J. Goree, Phys. Rev. E **50**, 2991 (1994).
[20] J. G. Kwak *et al.*, Phys. Plasmas **4**, 1463 (1997).
[21] R. Boswell, Plasma Phys. Controlled Fusion **26**, 1147 (1984).
[22] S. Cho, Phys. Plasmas **7**, 417 (2000).
[23] M. Porkalab, S. Bernabei, W. Hooke, R. Motely, and T. Nagashima, Phys. Rev. Lett. **38**, 230 (1977).
[24] M. Porkalab, V. Arunasalam, and R. A. Ellis, Jr., Phys. Rev. Lett. **29**, 1438 (1972).